

Contents

NMR Spectroscopy.....	S2
Relaxation theory.....	S3
1-D NMR Spectra for <i>cis</i> -dichlorobis(triphenylphosphine) platinum(II).....	S8
Relaxation measurements of <i>cis</i> - dichlorobis(triphenylphosphine) platinum(II).....	S9
Preparation of Silver complexes (2) and (3).....	S15
2-D NMR EXSY spectra for complexes (2) and (3).....	S16
References.....	S20

1. NMR Spectroscopy

NMR data were collected using a Bruker AVANCE III HD 400 MHz equipped with a BBO probe, Bruker AVANCE III HD 500MHz equipped with a BBFO SMART probe, a Bruker AVANCE III HD 600MHz with a BBO N₂-cooled Prodigy probe. Low VT experiments were carried out on the Bruker AVANCE III HD 500MHz over the range 203–298 K as stated using a Bruker liquid nitrogen evaporator VT system. Samples were dissolved in dry CD₂Cl₂, and CDCl₃ characterized by ³¹P{¹H}, 2D ³¹P-³¹P{¹H} COSY and ³¹P-³¹P{¹H} NOESY/EXSY (with proton decoupling throughout t₁ and t₂ acquisition periods), with exchange mixing times of 1ms to 10secs at the temperatures and in the solvents stated. For each data set, 8 or 16 transients were acquired for each of the 256 increments with 2K data points per FID, using a recovery time of 2 s. Data were processed typically as 1K × 1K data points using shifted squared-sinebell apodization windows. Typical sample concentrations for T₁ analyses were 0.05mM for Pt and 0.04 mM for Ag complexes based on silver(I) triflate. Probe temperature calibrations were performed using neat methanol samples (containing a trace of HCl) below ambient using either a BCU II cooling unit at 233K or a liquid nitrogen evaporator line at 203K.

³¹P T₁ Relaxation times were measured using the standard inversion-recovery sequence (180–*t*–90–acquire) in which *t* was varied from 5 ms to 10 s. Proton decoupling was applied during the acquisition period. Data were Fourier transformed using 2 Hz line broadening and relaxation times were calculated using the T₁ dynamics module in Topsin 3.5.

¹⁹⁵Pt T₁ Relaxation times were measured directly using the standard inversion-recovery sequence in which *t* was varied from 1 to 300 ms. Data were Fourier transformed using 2Hz line broadening and relaxation times were calculated using the T₁ dynamics module in Topsin 3.5.

2. Relaxation theory

2.1. Full *ab initio* Cross-relaxation Theory Treatment for two Spin -1/2 Particles in Solution

While it is intuitively clear that the change in the orientation of the coupled spin transfers the magnetisation from one doublet component to another, the abundance of complicated relaxation mechanisms in internally rigid systems featuring two CSA tensors and a dipolar coupling warrants closer attention. This section contains the complete *ab initio* analysis of every significant relaxation, cross-relaxation and cross-correlation process in a rigid system with two spin-1/2 particles dissolved in a liquid.

In the laboratory frame of reference, the most general case of the system in question would have the following spin Hamiltonian:

$$\begin{aligned}\hat{H}_{\text{iso}} &= \omega_L \hat{L}_Z + \omega_S \hat{S}_Z + 2\pi J \left[\hat{L}_X \hat{S}_X + \hat{L}_Y \hat{S}_Y + \hat{L}_Z \hat{S}_Z \right] \\ \hat{H}(t) &= \hat{H}_{\text{iso}} + \sum_{m,k=-2}^2 \mathfrak{D}_{km}^{(2)}(t) \hat{Q}_{km}\end{aligned}\quad (1)$$

where \hat{H}_{iso} is the orientation-independent part of the spin Hamiltonian, comprising Zeeman interaction terms with frequencies ω_L and ω_S , and the J -coupling. The orientation-dependent part is parameterised by the time-dependent second-rank Wigner functions $\mathfrak{D}_{km}^{(2)}(t)$ of molecular orientation and irreducible spherical components \hat{Q}_{km} of the anisotropic Hamiltonian, defined in the following way:

$$\hat{Q}_{km} = \Phi_m^{\text{CSA-L}} \hat{T}_k^{\text{L}} + \Phi_m^{\text{CSA-S}} \hat{T}_k^{\text{S}} + \Phi_m^{\text{DD}} \hat{T}_k^{\text{L,S}} \quad (2)$$

where the second-rank irreducible spherical tensor operators are

$$\begin{aligned}\hat{T}_0^{\text{L,S}} &= +\sqrt{\frac{2}{3}} \left(\hat{L}_Z \hat{S}_Z - \frac{1}{4} (\hat{L}_+ \hat{S}_- + \hat{L}_- \hat{S}_+) \right) \\ \hat{T}_{\pm 1}^{\text{L,S}} &= \mp \frac{1}{2} (\hat{L}_Z \hat{S}_{\pm} + \hat{L}_{\pm} \hat{S}_Z), \quad \hat{T}_{\pm 2}^{\text{L,S}} = +\frac{1}{2} \hat{L}_{\pm} \hat{S}_{\pm} \\ \hat{T}_0^{\text{S}} &= +\sqrt{\frac{2}{3}} \hat{S}_Z, \quad \hat{T}_{\pm 1}^{\text{S}} = \mp \frac{1}{2} \hat{S}_{\pm}, \quad \hat{T}_{\pm 2}^{\text{S}} = 0 \\ \hat{T}_0^{\text{L}} &= +\sqrt{\frac{2}{3}} \hat{L}_Z, \quad \hat{T}_{\pm 1}^{\text{L}} = \mp \frac{1}{2} \hat{L}_{\pm}, \quad \hat{T}_{\pm 2}^{\text{L}} = 0\end{aligned}\quad (3)$$

and the internal orientation parameters for the three interactions (CSA-L, CSA-S, DD) are

$$\begin{aligned}
\Phi_m^{\text{CSA-L}} &= \frac{Rh_L}{2} \left(\mathfrak{D}_{m,-2}^{(2)}(\alpha_L, \beta_L, \gamma_L) + \mathfrak{D}_{m,2}^{(2)}(\alpha_L, \beta_L, \gamma_L) \right) + \frac{Ax_L}{\sqrt{6}} \mathfrak{D}_{m,0}^{(2)}(\alpha_L, \beta_L, \gamma_L) \\
\Phi_m^{\text{CSA-S}} &= \frac{Rh_S}{2} \left(\mathfrak{D}_{m,-2}^{(2)}(\alpha_S, \beta_S, \gamma_S) + \mathfrak{D}_{m,2}^{(2)}(\alpha_S, \beta_S, \gamma_S) \right) + \frac{Ax_S}{\sqrt{6}} \mathfrak{D}_{m,0}^{(2)}(\alpha_S, \beta_S, \gamma_S) \\
\Phi_m^{\text{D}} &= \frac{Rh_D}{2} \left(\mathfrak{D}_{m,-2}^{(2)}(\alpha_D, \beta_D, \gamma_D) + \mathfrak{D}_{m,2}^{(2)}(\alpha_D, \beta_D, \gamma_D) \right) + \frac{Ax_D}{\sqrt{6}} \mathfrak{D}_{m,0}^{(2)}(\alpha_D, \beta_D, \gamma_D)
\end{aligned} \tag{4}$$

where the three sets of Euler angles $\{\alpha, \beta, \gamma\}$ specify the orientations of the corresponding interactions in the molecular frame of reference; axiality and rhombicity parameters of the three interactions are:

$$\begin{aligned}
Ax_L &= -\gamma_L B_Z \left[2\sigma_{ZZ}^L - (\sigma_{XX}^L + \sigma_{YY}^L) \right], & Rh_L &= -\gamma_L B_Z (\sigma_{XX}^L - \sigma_{YY}^L) \\
Ax_S &= -\gamma_S B_Z \left[2\sigma_{ZZ}^S - (\sigma_{XX}^S + \sigma_{YY}^S) \right], & Rh_S &= -\gamma_S B_Z (\sigma_{XX}^S - \sigma_{YY}^S) \\
Ax_D &= -6 \frac{\mu_0}{4\pi} \frac{\gamma_L \gamma_S \hbar}{r_{LS}^3}, & Rh_D &= 0
\end{aligned} \tag{5}$$

where $\gamma_{L,S}$ are the magnetogyric ratios of the two spins, $\{\sigma_{XX}^{L,S}, \sigma_{YY}^{L,S}, \sigma_{ZZ}^{L,S}\}$ are eigenvalues of their chemical shift tensors, and r_{LS} is the distance between them. A very detailed derivation of this form of the spin Hamiltonian is available in Section 2 of IK's paper on the subject [1]; a general numerical implementation is available in *Spinach* [2].

The general Liouville space form of the Bloch-Redfield-Wangsness relaxation superoperator $\hat{\hat{R}}$ for the case of rotationally modulated interactions is [1,3]:

$$\hat{\hat{R}} = - \sum_{kmpq} \int_0^\infty G_{kmpq}(\tau) \hat{\hat{Q}}_{km} e^{-i\hat{H}_0\tau} \hat{\hat{Q}}_{pq}^\dagger e^{i\hat{H}_0\tau} d\tau \tag{6}$$

where the rotational correlation functions $G_{kmpq}(\tau)$ are ensemble averages of the products of differently timed Wigner functions from Equation (1):

$$G_{kmpq}(\tau) = \left\langle \mathfrak{D}_{km}^{(2)}(0) \mathfrak{D}_{pq}^{(2)*}(\tau) \right\rangle \tag{7}$$

We shall assume isotropic rotational diffusion in for the system in question, in which case

$$G_{abcd}(\tau) = \frac{\delta_{a,c} \delta_{b,d}}{5} e^{-\frac{\tau}{\tau_c}} \tag{8}$$

where δ denotes Kronecker symbols and τ_c is the rotational correlation time.

Despite its complicated definition, the integral in Equation (6) may be evaluated analytically in a closed form by symbolic algebra packages, such as *Mathematica* [4]. Here we focus on the specific

matrix element that corresponds to the longitudinal relaxation and cross-relaxation between the two doublet components of the spin being detected.

Under the assumptions specified above and neglecting the dynamic frequency shifts, the longitudinal self-relaxation rates for the two spins (expressed for the low- γ S spin as $R_1[S]$ in the main paper text) are:

$$\frac{\langle \hat{L}_Z | \hat{R} | \hat{L}_Z \rangle}{\langle \hat{L}_Z | \hat{L}_Z \rangle} = -\frac{\Delta_{\text{CSA-L}}^2}{30} J(\tau_c, \omega_L) - \frac{\Delta_{\text{DD}}^2}{360} [3J(\tau_c, \omega_L) + J(\tau_c, \omega_L - \omega_s) + 6J(\tau_c, \omega_L + \omega_s)]$$

$$\frac{\langle \hat{S}_Z | \hat{R} | \hat{S}_Z \rangle}{\langle \hat{S}_Z | \hat{S}_Z \rangle} = -\frac{\Delta_{\text{CSA-S}}^2}{30} J(\tau_c, \omega_s) - \frac{\Delta_{\text{DD}}^2}{360} [3J(\tau_c, \omega_s) + J(\tau_c, \omega_L - \omega_s) + 6J(\tau_c, \omega_L + \omega_s)]$$
(9)

where the angular brackets denote the Frobenius scalar product $\langle \hat{A} | \hat{B} \rangle = \text{Tr}[\hat{A}^\dagger \hat{B}]$ and the squared modulation depth parameters are defined as

$$\Delta_A^2 = Ax_A^2 + 3Rh_A^2$$
(10)

and the spectral power density function is

$$J(\tau, \omega) = \frac{\tau}{1 + \omega^2 \tau^2}$$
(11)

These are standard results that match the literature [5].

The eigenstates of the Zeeman Hamiltonian that represent the left and the right components of the weakly coupled L spin doublet are linear combinations of in-phase and anti-phase magnetisation:

$$\hat{M}_{\text{left}}^L = \hat{L}_Z - 2\hat{L}_Z \hat{S}_Z \quad \hat{M}_{\text{right}}^L = \hat{L}_Z + 2\hat{L}_Z \hat{S}_Z$$
(12)

The longitudinal cross-relaxation rate between these states (expressed as $R_{\text{SE}}[L]$ in the main paper text) is:

$$\frac{\langle \hat{M}_{\text{left}}^L | \hat{R} | \hat{M}_{\text{right}}^L \rangle}{\sqrt{\langle \hat{M}_{\text{left}}^L | \hat{M}_{\text{left}}^L \rangle \langle \hat{M}_{\text{right}}^L | \hat{M}_{\text{right}}^L \rangle}} =$$

$$= \frac{\Delta_{\text{CSA-S}}^2}{60} J(\tau_c, \omega_s) + \frac{\Delta_{\text{DD}}^2}{720} [3J(\tau_c, \omega_s) - J(\tau_c, \omega_L - \omega_s) - 6J(\tau_c, \omega_L + \omega_s)]$$
(13)

It is a considerable relief to observe that, after a fully general relaxation theory treatment, no CSA-CSA or DD-CSA cross-correlation contributions are predicted in this cross-relaxation rate – the only terms are the intuitively obvious CSA relaxation of the partner spin and the Overhauser style cross-relaxation.

It is clear from Equations (9) and (13) that the L spin satellite cross-relaxation rate is equal to half the relaxation rate of the S spin only in the circumstances when the dipolar terms are negligible:

$$\frac{\langle \hat{S}_Z | \hat{R} | \hat{S}_Z \rangle}{\langle \hat{S}_Z | \hat{S}_Z \rangle} \approx -\frac{\Delta_{\text{CSA-S}}^2}{30} J(\tau_c, \omega_s)$$

$$\frac{\langle \hat{M}_{\text{left}}^L | \hat{R} | \hat{M}_{\text{right}}^L \rangle}{\sqrt{\langle \hat{M}_{\text{left}}^L | \hat{M}_{\text{left}}^L \rangle \langle \hat{M}_{\text{right}}^L | \hat{M}_{\text{right}}^L \rangle}} \approx \frac{\Delta_{\text{CSA-S}}^2}{60} J(\tau_c, \omega_s) \quad (14)$$

The presence of $\gamma_L^2 \gamma_S^2$ term in Δ_{DD}^2 makes this easy to demonstrate for ^{31}P - ^{107}Ag and ^{31}P - ^{109}Ag systems in non-viscous liquids at high magnetic fields. The direct bond is longer than 2 Angstroms, and therefore

$$\frac{\Delta_{\text{DD}}^2}{360} [3J(\tau_c, \omega_L) + J(\tau_c, \omega_L - \omega_s) + 6J(\tau_c, \omega_L + \omega_s)] < 10^{-3} \text{ s}^{-1} \quad (15)$$

in a 9.4 Tesla magnet for a compound with $\tau_c = 200$ ps – negligible compared to the experimentally observed relaxation rates, which are therefore entirely due to the CSA mechanism.

The conclusion is that the cross-relaxation rate measured on the metal satellites of the observed NMR signal is half the longitudinal relaxation rate of the metal spin. This applies to any system in which the CSA mechanism dominates relaxation; that includes most low- γ nuclei with spin 1/2, the only exception likely being molecules with very high symmetry at the low- γ nucleus.

2.2. Chemical shift tensor and relaxation time calculations

Molecular geometries were optimised in *Gaussian09* [6] using M06 exchange-correlation functional [7] with cc-pVDZ basis set [8] on C, H, O atoms, 6-31G(d) basis set on phosphorus[9], and aug-cc-pVTZ-PP basis set [10] on silver. SMD solvent model [11] was used to account for the influence of the dichloromethane solvent. The resulting geometries were used for GIAO [12] calculations of chemical shielding tensors using the same exchange correlation functional and basis sets. Longitudinal relaxation rates were computed in *Spinach* [1] using the diagonalization-free version [2] of Bloch-Redfield-Wangsness formalism [13-15] from the resulting molecular geometries and shielding tensors. Rotational diffusion tensors for the two complexes in dichloromethane ($\eta = 1.61$ cP at 203 K) were computed in *HYDRONMR* [16] using the bead model [17]. Both rotational diffusion tensors were found to be nearly isotropic – eigenvalues 82, 85, 90 MHz for the bigger silver complex **2**, and 93, 97, 107 MHz for the smaller silver complex **3**, corresponding to the isotropic rotational correlation times of 1.9 ns and 1.7 ns, respectively.

Longitudinal relaxation times may be estimated using BRW theory from DFT estimates of silver chemical shielding tensors and hydrodynamic radii. Because relaxation times depend quadratically on

CSA eigenvalues and cubically on the effective hydrodynamic radius, the calculations should be viewed as order-of-magnitude estimates. Analytical equations, including the rarely acknowledged contributions from the antisymmetric parts of the shielding tensors, are given below, ω_N is nuclear Zeeman frequency.

$$\begin{aligned} R_1 &= \frac{1}{2} \Lambda_\sigma^2 \omega_N^2 \frac{\tau_R}{1 + 9\omega_N^2 \tau_R^2} + \frac{2}{15} \Delta_\sigma^2 \omega_N^2 \frac{\tau_R}{1 + \omega_N^2 \tau_R^2} \\ R_2 &= \frac{1}{4} \Lambda_\sigma^2 \omega_N^2 \frac{\tau_R}{1 + 9\omega_N^2 \tau_R^2} + \frac{1}{45} \Delta_\sigma^2 \omega_N^2 \left(4\tau_R + \frac{3\tau_R}{1 + \omega_N^2 \tau_R^2} \right) \end{aligned} \quad (16)$$

where Λ_σ^2 is the first rank invariant (asymmetry squared) of the total chemical shift tensor:

$$\Lambda_\sigma^2 = (\sigma_{XY} - \sigma_{YX})^2 + (\sigma_{XZ} - \sigma_{ZX})^2 + (\sigma_{YZ} - \sigma_{ZY})^2 \quad (17)$$

and Δ_σ^2 is the second rank invariant (anisotropy squared) of the total chemical shift tensor:

$$\begin{aligned} \Delta_\sigma^2 &= \sigma_{XX}^2 + \sigma_{YY}^2 + \sigma_{ZZ}^2 - \sigma_{XX}\sigma_{YY} - \sigma_{XX}\sigma_{ZZ} - \sigma_{YY}\sigma_{ZZ} + \\ &+ \frac{3}{4} \left[(\sigma_{XY} + \sigma_{YX})^2 + (\sigma_{XZ} + \sigma_{ZX})^2 + (\sigma_{YZ} + \sigma_{ZY})^2 \right] \end{aligned} \quad (18)$$

In practice, the Gaussian09 logs are read directly into *Spinach*, and relaxation theory analysis including dipolar and CSA mechanisms is performed automatically as described in [1]. The resulting numerical data is given in Tables S1 and S2 below.

Table S1: Calculated relaxation times for the bigger silver complex (**2**), $\tau_C=1.9$ ns from HYDRONMR.

Isotope	R_1 / s^{-1}	R_2 / s^{-1}	T_1 / s	T_2 / s
^{109}Ag	0.012	0.014	86	72
^{31}P	0.20	0.91	5.0	1.1
^{31}P	0.20	0.91	5.0	1.1
^{31}P	0.20	0.91	5.0	1.1
^{31}P	0.20	0.91	5.0	1.1

Table S2: Calculated relaxation times for the smaller silver complex (**3**), $\tau_C=1.7$ ns from HYDRONMR.

Isotope	R_1 / s^{-1}	R_2 / s^{-1}	T_1 / s	T_2 / s
^{109}Ag	0.050	0.059	20	17
^{31}P	0.26	0.93	3.9	1.1
^{31}P	0.22	0.79	4.5	1.6

The doublet component cross-relaxation rate for the bigger complex is predicted to be $0.0054 s^{-1}$, and $0.0242 s^{-1}$ for the smaller complex. In both cases, the analytical insight is confirmed by numerical simulations – the doublet component cross-relaxation rate (i.e. satellite exchange rate) is exactly half the silver longitudinal relaxation rate.

3. 1-D NMR Spectra for *cis*-dichlorobis(triphenylphosphine) platinum(II)

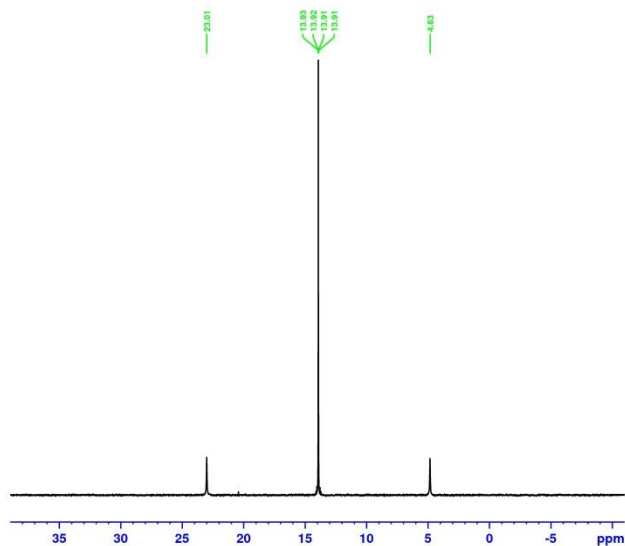


Figure S1: ^{31}P { ^1H } NMR Spectrum of *cis*-dichlorobis(triphenylphosphine) platinum(II) (50 mM) in CD_2Cl_2 at 500 MHz (^1H) and 298 K (LB = 2 Hz)

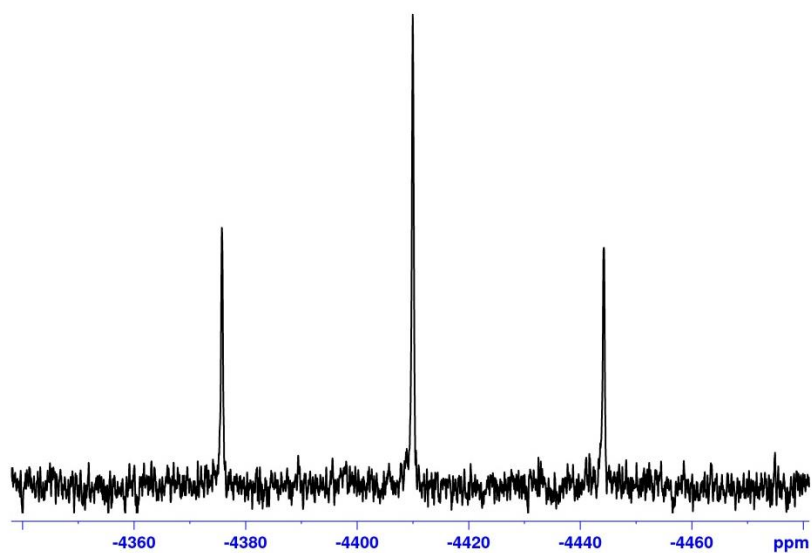


Figure S2: ^{195}Pt NMR Spectrum of *cis*-dichlorobis(triphenylphosphine) platinum(II) (50 mM) in CD_2Cl_2 at 500 MHz (^1H) 298K (LB =10 Hz)

4. Relaxation measurements of *cis*- dichlorobis(triphenylphosphine) platinum(II)

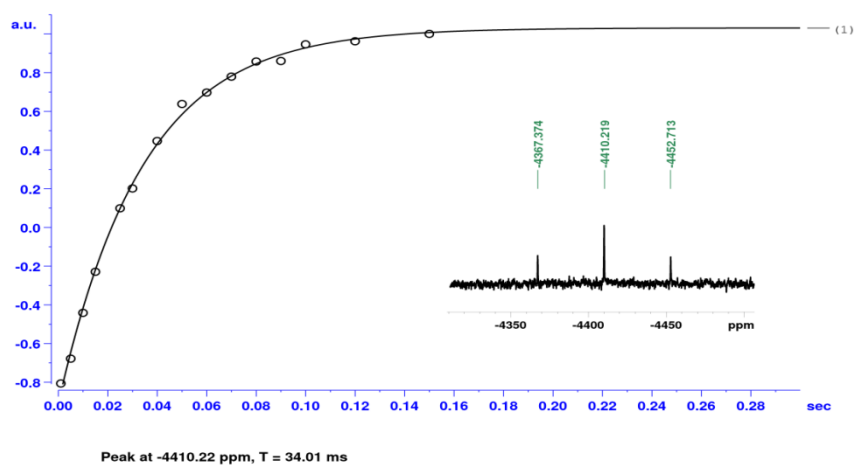


Figure S3: ^{195}Pt T_1 Relaxation measurement using the standard inversion-recovery sequence for *cis*-dichlorobis(triphenylphosphine) platinum(II) at 9.4 T (400 MHz ^1H).

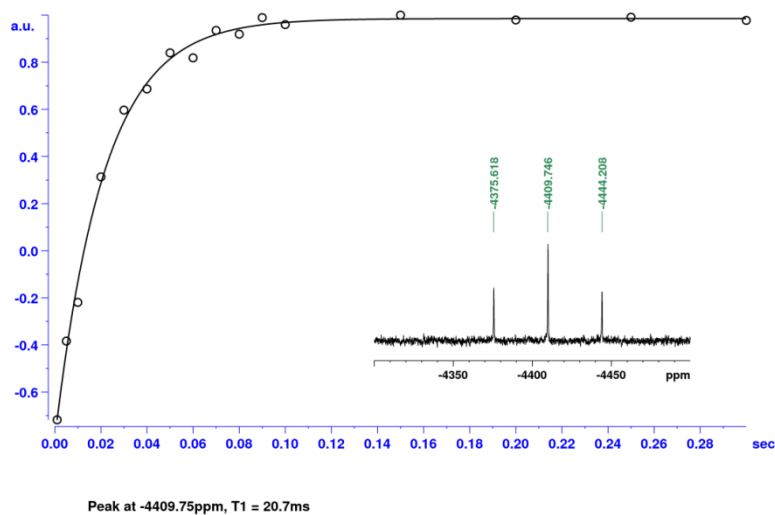


Figure S4: ^{195}Pt T_1 Relaxation measurement using the standard inversion-recovery sequence for *cis*-dichlorobis(triphenylphosphine) platinum(II) at 11.74 T (500 MHz ^1H).

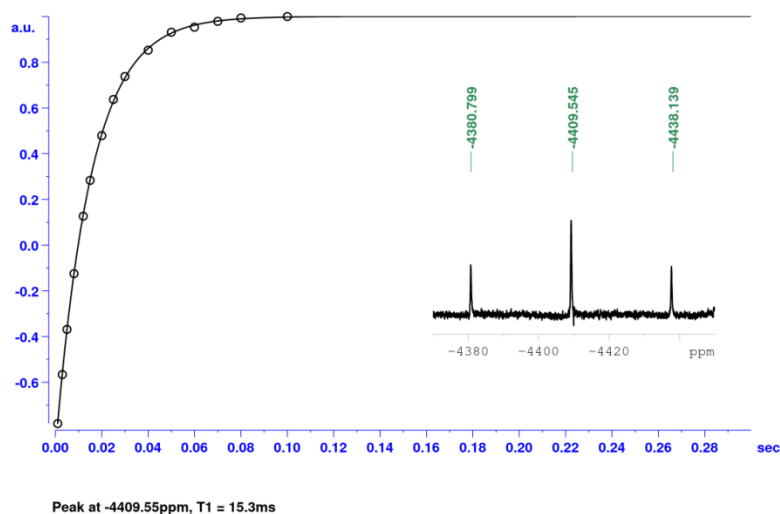


Figure S5: ^{195}Pt T_1 Relaxation measurement using the standard inversion-recovery sequence for *cis*-dichlorobis(triphenylphosphine) platinum(II) at 14.09 T (600 MHz ^1H).

B_0/T (^1H MHz)	$T_1(^{31}\text{P})/\text{sec}$
9.40 (400MHz)	5.05
11.74 (500MHz)	3.85
14.09 (600 MHz)	2.91

Table S3: ^{31}P longitudinal relaxation times for *cis*-dichlorobis(triphenylphosphine) platinum(II) from inversion recovery experiments.

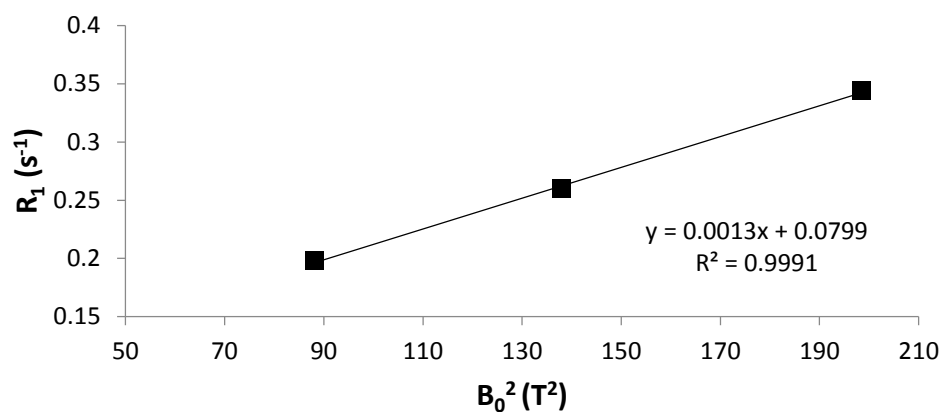


Figure S6: Relaxation rate dependence of ^{31}P in *cis*-dichlorobis(triphenylphosphine) platinum(II) on the square of the applied magnetic field B_0 .

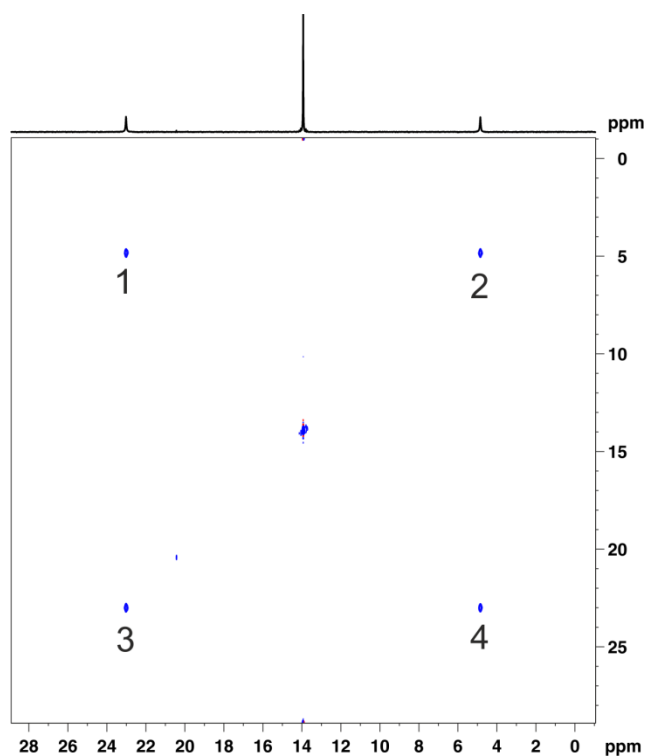


Figure S7: Integral numbering system used for the ^{195}Pt -satellite peaks in the ^{31}P EXSY spectrum. A ratio of integral 1: integral 2 was recorded ($I_{\text{cross-peak}}/I_{\text{diagonal}}$) and plotted against mixing time to yield data in Figure 2 of main paper. The same analysis was performed for integral 4 with respect to integral 3, which produced similar results (see Figure S8).

tmix/msec	Volume 1	Volume 2	Volume 3	Volume 4	Normalise (1/2)	Normalise (4/3)
2	605630	18944000	18460000	498650	0.031969489	0.027012459
5	1510700	17708000	17730000	1335100	0.085311724	0.075301748
6	1718200	18294000	18012000	1761700	0.093921504	0.097807018
8	2304000	17716000	17949000	2313800	0.13005193	0.128909689
10	2201200	16008000	16483000	2422700	0.137506247	0.146981739
12	3288000	17110000	17009000	3254900	0.192168323	0.191363396
15	3440500	15793000	15232000	3612900	0.21784968	0.237191439
20	3973600	14208000	14120000	3905300	0.279673423	0.27657932
25	5029100	14336000	14217000	5555100	0.350802176	0.390736442
30	5410500	13022000	12685000	5513000	0.415489172	0.434607804

Table S4: Volume integrals of ^{195}Pt -satellite cross peaks (1,4) normalised against the diagonal peaks (2,3) for *cis*-dichlorobis(triphenylphosphine) platinum(II) ^{195}Pt satellite cross-relaxation measurement using ^{31}P - ^{31}P - $\{^1\text{H}\}$ -EXSY spectra at 400 MHz (^1H) at 298K.

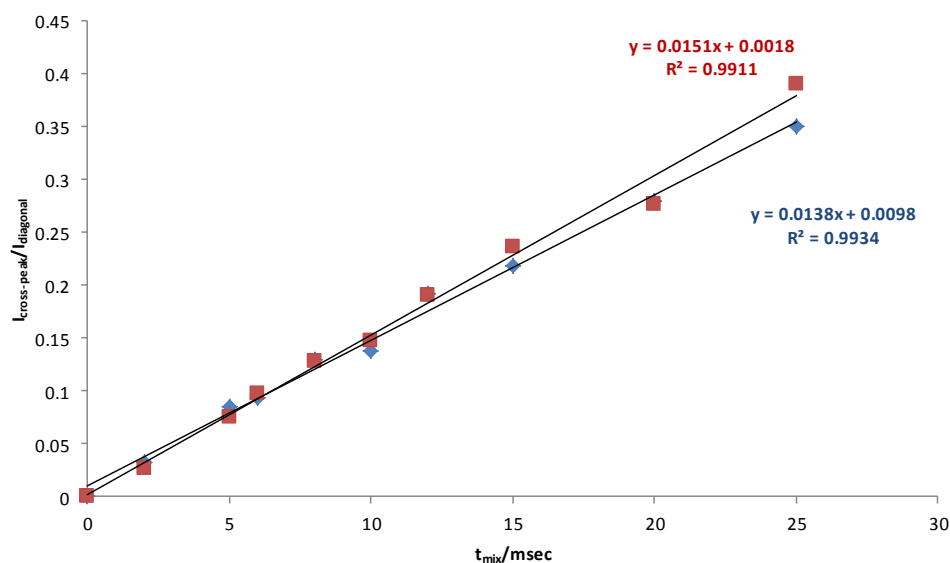


Figure S8: Normalised volume integrals for satellite peak 1 with respect to diagonal peak 2 (blue points) and normalised volume integrals for satellite peak 4 with respect to diagonal peak 3 (red points) in ^{31}P EXSY recorded at 400 MHz (^1H), 298 K.

tmix/msec	Volume 1	Volume 2	Volume 3	Volume 4	Normalise (1/2)	Normalise (4/3)
1	33288	4200600	4206400	72765	0.007924582	0.01729864
2	167120	4303500	4163800	157360	0.038833508	0.037792401
3	402230	4439100	4500700	159650	0.090610709	0.03547226
4	346260	3970300	4034900	343290	0.087212553	0.085080175
5	412780	4073200	3952000	495450	0.101340469	0.125366903
6	437050	3934000	3910700	462800	0.111095577	0.118341985
7	562260	3989800	4016800	615020	0.140924357	0.15311193
8	682420	3715600	3759200	711980	0.183663473	0.18939668
10	749740	3443500	3483900	718340	0.217726151	0.206188467
12	1009500	3425300	3447100	997750	0.294718711	0.289446201
15	1089700	3258100	3415500	1075700	0.334458734	0.314946567
18	1318600	3323600	3453700	1314300	0.396738476	0.380548397
20	1381200	3160600	3034200	1359600	0.437005632	0.448091754
25	1601600	2935500	2952600	1552700	0.545597002	0.5258755
30	1628400	2538300	2598500	1639400	0.641531734	0.630902444

Table S5: Volume integrals of ^{195}Pt -satellite cross peaks (1,4) normalised against the diagonal peaks (2,3) for *cis*-dichlorobis(triphenylphosphine) platinum(II) ^{195}Pt satellite cross-relaxation measurement using ^{31}P - ^{31}P - $\{^1\text{H}\}$ -EXSY spectra at 500 MHz (^1H) and 298 K.

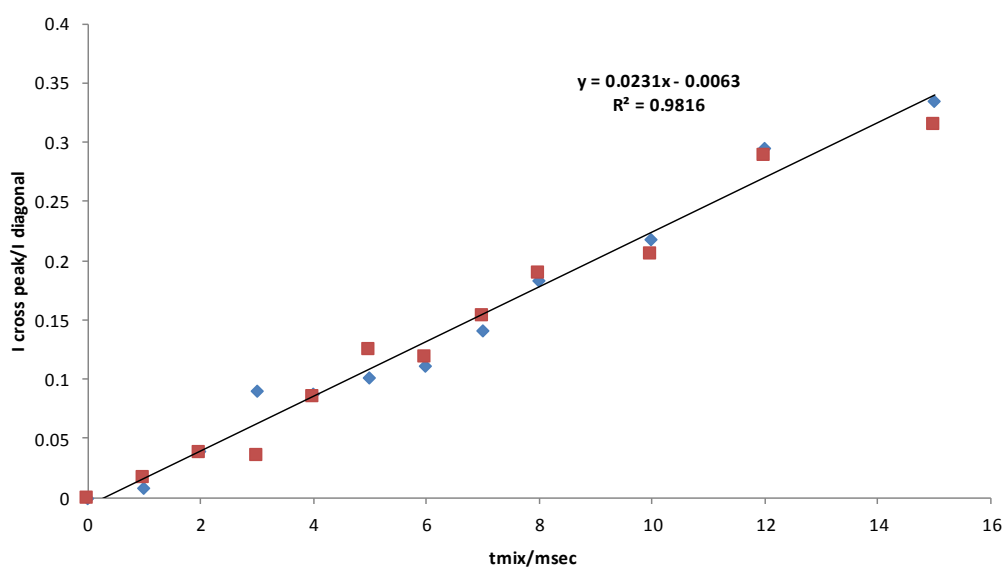


Figure S9: Normalised volume integrals for satellite peak 1 with respect to diagonal peak 2 (blue points) and for satellite peak 4 with respect to diagonal peak 3 (red points) in ^{31}P EXSY recorded at 500 MHz (^1H), 298 K.

t _{mix} /msec	Volume 1	Volume 2	Volume 3	Volume 4	Normalise (1/2)	Normalise (4/3)
1	579590	19474000	19308000	799780	0.029762247	0.041422208
2	1461700	19020000	19196000	1387300	0.076850683	0.072270265
4	2327100	19086000	18729000	2459000	0.121927067	0.131293716
6	3456200	18153000	17969000	3542600	0.190392773	0.197150648
8	4334600	17233000	17185000	4315300	0.251529043	0.251108525
10	5068700	16284000	16199000	4994000	0.31126873	0.308290635
12	5645400	15352000	15200000	5876100	0.367730589	0.386585526
15	6730900	14814000	14555000	6601400	0.45436074	0.453548609
20	7771100	13692000	13589000	7721700	0.567565001	0.568231658
25	8742400	12893000	12918000	8668000	0.678073373	0.671001703
30	14119000	18892000	18585000	14131000	0.747353377	0.760344364

Table S6: Volume integrals of ^{195}Pt -satellite cross peaks (1,4) normalised against the diagonal peaks (2,3) for *cis*-dichlorobis(triphenylphosphine) platinum(II) ^{195}Pt satellite cross-relaxation measurement using ^{31}P - ^{31}P - $\{^1\text{H}\}$ -EXSY spectra at 600 MHz (^1H) at 298K.

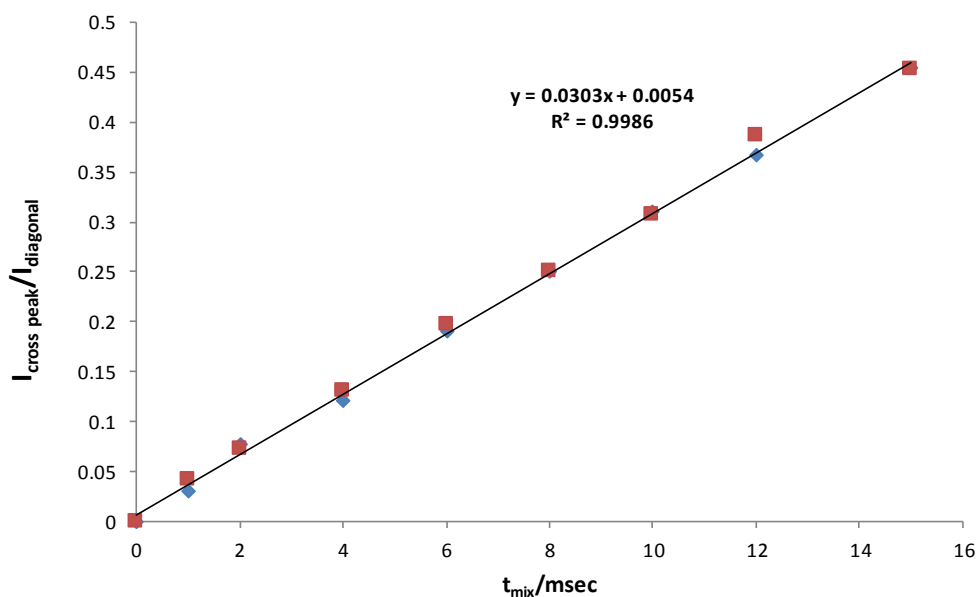


Figure S10: Normalised volume integrals for satellite peak 1 with respect to diagonal peak 2 (blue points) and normalised volume integrals for satellite peak 4 with respect to diagonal peak 3 (red points) at 600 MHz (^1H), 298 K.

5. Preparation of Silver complexes (2) and (3)

5.1 General Procedure for preparation of Silver(I) complexes (2) and (3)

A 10 mL round bottom flask was charged with silver(I) triflate (9 mg, 0.035 mmol, 1.0 equiv) and (R)-(+)-5,5'-Bis[di(3,5-xylyl)phosphino]-4,4'-bi-1,3-benzodioxole (50 mg, 0.07 mmol, 2.0 equiv). Under argon, CDCl_3 or CD_2Cl_2 (0.8 mL) was added and the mixture was stirred for 30 minutes at room temperature. The solution was then transferred to an NMR tube for analysis.

5.2 1-D NMR spectra for complexes (2) and (3)

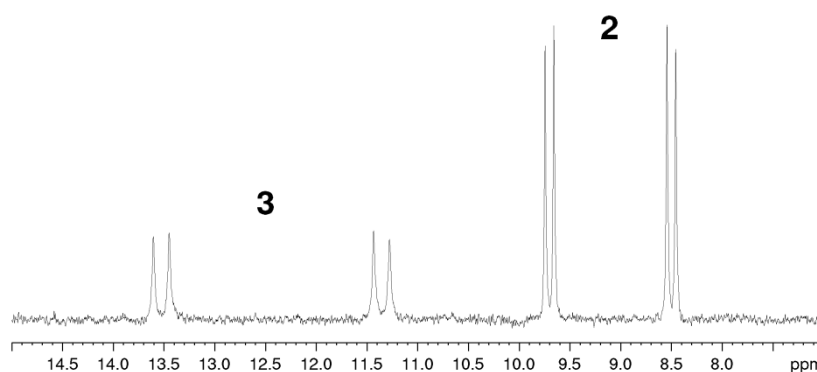


Figure S11: ^{31}P { ^1H } NMR Spectrum of silver complexes (2) and (3) (40 mM) in CDCl_3 at 233 K and 500 MHz (^1H) (LB = 1 Hz).

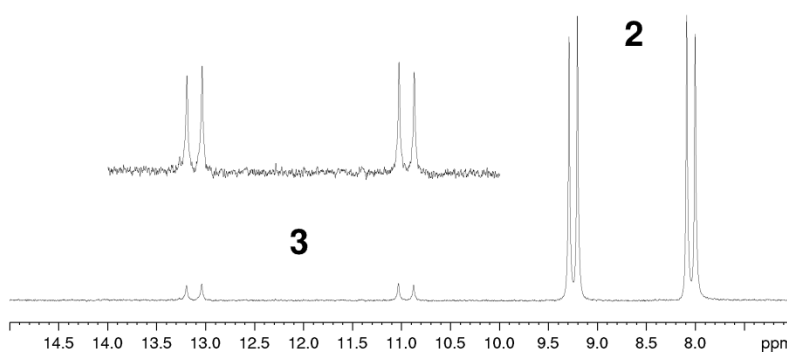
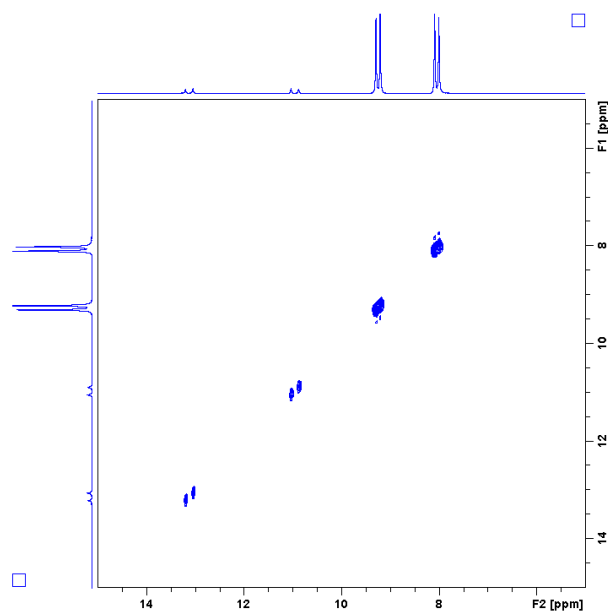


Figure S12: ^{31}P { ^1H } NMR Spectrum of silver complexes (2) and (3) (40 mM) in CD_2Cl_2 at 203 K and 500 MHz (^1H) (LB = 1 Hz)

6. 2-D NMR EXSY spectra for complexes (2) and (3)

a)



b)

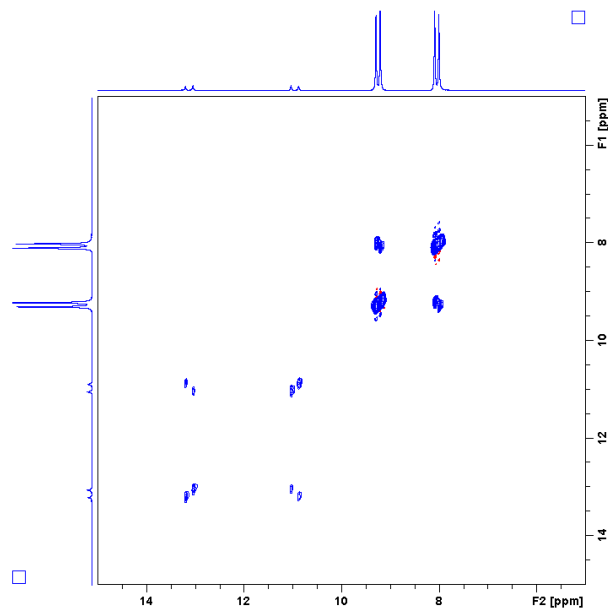


Figure S13: ^{31}P - ^{31}P - $\{^1\text{H}\}$ -EXSY spectra of (2) and (3) showing the $^{107/109}\text{Ag}$ satellite cross-peak appearance as function of t_{mix} (a) 10 ms (b) 500 ms (CD_2Cl_2 , 203 K, 500 MHz (^1H)).

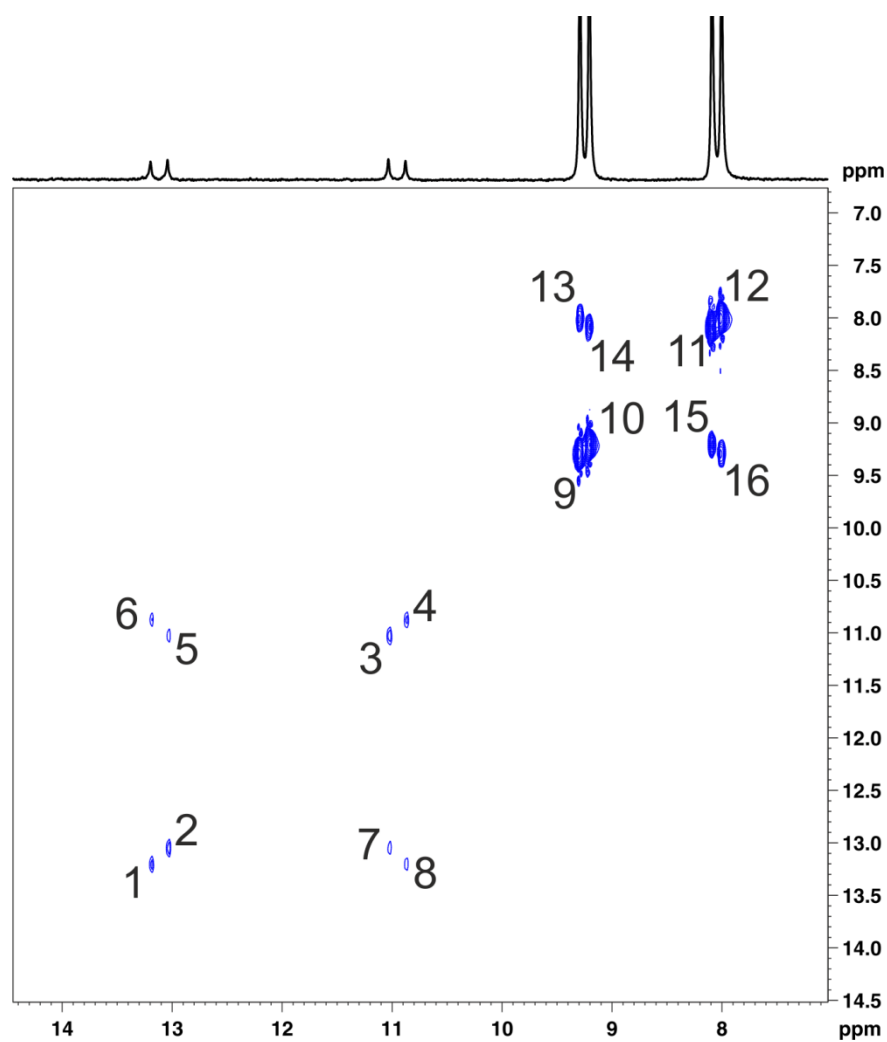


Figure S14: Integral numbering system used for the Ag-satellite peaks in the ^{31}P EXSY spectrum. For trigonal-planar complex (**3**), a ratio of volume integral 6:4 was taken for ^{109}Ag satellites, and 5:3 for ^{107}Ag satellites. For tetrahedral complex (**2**), a ratio of volume integral 13:12 was taken for ^{109}Ag satellites.

tmix/msec	Volume 3	Volume 4	Volume 5	Volume 6	Normalise ^{31}P - ^{107}Ag	Normalise ^{31}P - ^{109}Ag
50	1256700	1132800	64787	66323	0.051553274	0.058547846
75	1131400	1095900	89107	86178	0.078758176	0.078636737
100	1103300	1014100	80230	123560	0.072718209	0.121842027
200	912070	822820	159470	195130	0.174844036	0.237147857
300	743940	650210	194640	266020	0.261634003	0.409129358
400	610840	507970	232320	245270	0.380328728	0.482843475
500	490730	420910	188070	223610	0.383245369	0.531253712
600	412970	344310	188900	207710	0.457418214	0.6032645
700	329670	326720	230290	234100	0.698547032	0.716515671
800	287430	230060	205640	188880	0.71544376	0.821003217

Table S7: ^{31}P EXSY peak volume data for trigonal planar complex (**3**).

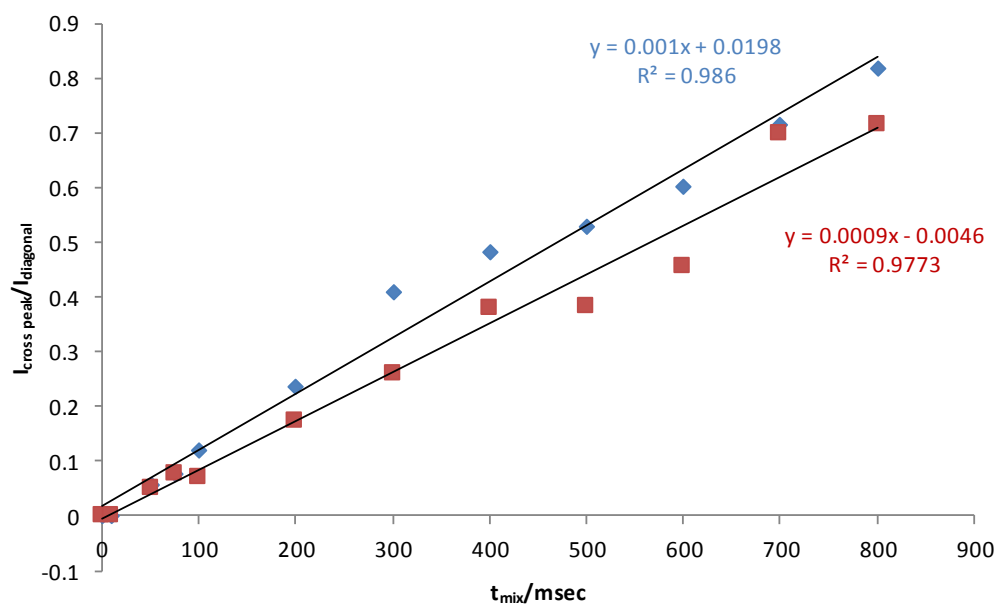


Figure S15: Normalised volume integrals for trigonal planar complex (**3**) at 500 MHz (^{107}Ag satellite 5:3 (red points), ^{109}Ag satellite 6:4 (blue points)).

tmix/msec	Volume 11	Volume 12	Volume 13	Volume 14	Normalise ³¹ P- ¹⁰⁷ Ag	Normalise ³¹ P- ¹⁰⁹ Ag
50	18305000	17194000	131760	144370	0.007886916	0.007663138
75	17452000	16861000	200280	168600	0.009660784	0.011878299
100	17774000	16643000	223890	216310	0.012170024	0.013452503
200	16906000	15582000	448880	409600	0.024228085	0.028807599
300	15352000	15667000	627770	496780	0.032359302	0.040069573
400	15207000	14082000	805150	688820	0.045296245	0.057175827
500	11710000	14457000	813750	746140	0.06371819	0.056287612
600	10954000	12327000	888150	800150	0.073046376	0.07204916
700	10215000	13489000	833790	901950	0.088296623	0.061812588
800	12161000	11226000	1086600	902790	0.074236494	0.096793159

Table S8: ³¹P EXSY peak volume data for tetrahedral complex (**2**).

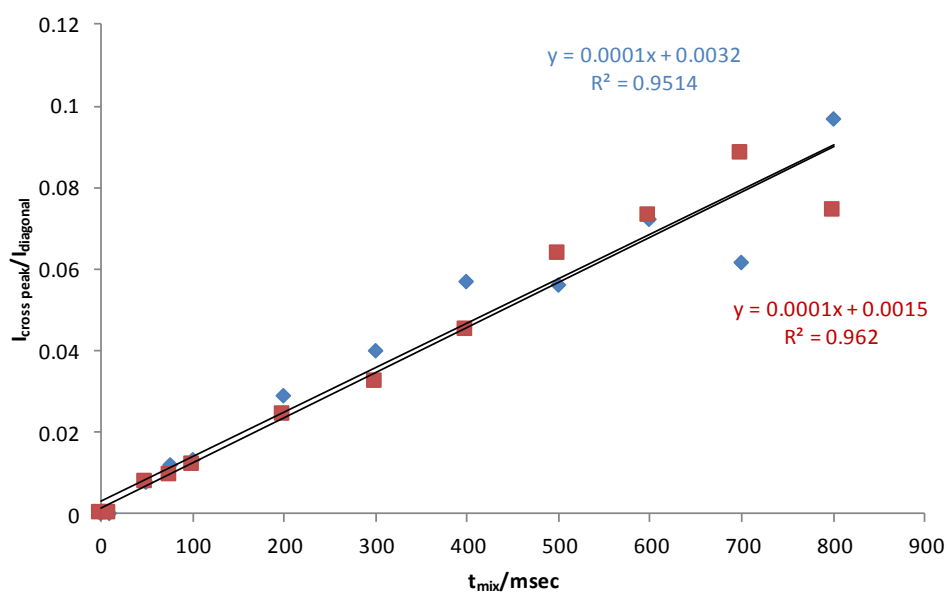


Figure S16: Normalised volume integrals for tetrahedral complex (**2**) at 500 MHz (¹⁰⁷Ag satellite 14:11 (red points), ¹⁰⁹Ag satellite 13:12 (blue points)).

7. References

- [1] I. Kuprov, Diagonalization-free implementation of spin relaxation theory for large spin systems, *Journal of Magnetic Resonance*, 209 (2011) 31-38.
- [2] H. Hogben, M. Krzystyniak, G. Charnock, P. Hore, I. Kuprov, Spinach – a software library for simulation of spin dynamics in large spin systems, *Journal of Magnetic Resonance*, 208 (2011) 179-194.
- [3] S. Szymanski, A.M. Gryff-Keller, G. Binsch, A liouville space formulation of wangsness-bloch-redfield theory of nuclear spin relaxation suitable for machine computation. I. fundamental aspects, *Journal of Magnetic Resonance*, 68 (1986) 399-432.
- [4] I. Kuprov, N. Wagner-Rundell, P. Hore, Bloch-Redfield-Wangsness theory engine implementation using symbolic processing software, *Journal of Magnetic Resonance*, 184 (2007) 196-206.
- [5] M. Goldman, Interference effects in the relaxation of a pair of unlike spin-1/2 nuclei, *Journal of Magnetic Resonance*, 60 (1984) 437-452.
- [6] M.J. Frisch, G.W. Trucks, H.B. Schlegel, G.E. Scuseria, M.A. Robb, J.R. Cheeseman, G. Scalmani, V. Barone, B. Mennucci, G.A. Petersson, H. Nakatsuji, M. Caricato, X. Li, H.P. Hratchian, A.F. Izmaylov, J. Bloino, G. Zheng, J.L. Sonnenberg, M. Hada, M. Ehara, K. Toyota, R. Fukuda, J. Hasegawa, M. Ishida, T. Nakajima, Y. Honda, O. Kitao, H. Nakai, T. Vreven, J.A. Montgomery Jr., J.E. Peralta, F. Ogliaro, M.J. Bearpark, J. Heyd, E.N. Brothers, K.N. Kudin, V.N. Staroverov, R. Kobayashi, J. Normand, K. Raghavachari, A.P. Rendell, J.C. Burant, S.S. Iyengar, J. Tomasi, M. Cossi, N. Rega, N.J. Millam, M. Klene, J.E. Knox, J.B. Cross, V. Bakken, C. Adamo, J. Jaramillo, R. Gomperts, R.E. Stratmann, O. Yazyev, A.J. Austin, R. Cammi, C. Pomelli, J.W. Ochterski, R.L. Martin, K. Morokuma, V.G. Zakrzewski, G.A. Voth, P. Salvador, J.J. Dannenberg, S. Dapprich, A.D. Daniels, Ö. Farkas, J.B. Foresman, J.V. Ortiz, J. Cioslowski, D.J. Fox, *Gaussian 09*, in, Gaussian, Inc., Wallingford, CT, USA, 2009.
- [7] Y. Zhao, D.G. Truhlar, The M06 suite of density functionals for main group thermochemistry, thermochemical kinetics, noncovalent interactions, excited states, and transition elements: two new functionals and systematic testing of four M06-class functionals and 12 other functionals, *Theoretical Chemistry Accounts*, 120 (2008) 215-241.
- [8] T.H. Dunning Jr, Gaussian basis sets for use in correlated molecular calculations. I. The atoms boron through neon and hydrogen, *The Journal of Chemical Physics*, 90 (1989) 1007-1023.

- [9] W.J. Hehre, R. Ditchfield, J.A. Pople, Self-consistent molecular orbital methods. XII. Further extensions of gaussian-type basis sets for use in molecular orbital studies of organic molecules, *The Journal of Chemical Physics*, 56 (1972) 2257-2261.
- [10] K.A. Peterson, C. Puzzarini, Systematically convergent basis sets for transition metals. II. Pseudopotential-based correlation consistent basis sets for the group 11 (Cu, Ag, Au) and 12 (Zn, Cd, Hg) elements, *Theoretical Chemistry Accounts: Theory, Computation, and Modelling (Theoretica Chimica Acta)*, 114 (2005) 283-296.
- [11] A.V. Marenich, C.J. Cramer, D.G. Truhlar, Universal Solvation Model Based on Solute Electron Density and on a Continuum Model of the Solvent Defined by the Bulk Dielectric Constant and Atomic Surface Tensions, *The Journal of Physical Chemistry B*, 113 (2009) 6378-6396.
- [12] F. London, Théorie quantique des courants interatomiques dans les combinaisons aromatiques, *J. Phys. Radium*, 8 (1937) 397-409.
- [13] M. Goldman, Formal theory of spin-lattice relaxation, *Journal of Magnetic Resonance*, 149 (2001) 160-187.
- [14] A.G. Redfield, On the theory of relaxation processes, *IBM Journal of Research and Development*, 1 (1957) 19-31.
- [15] R.K. Wangsness, F. Bloch, The dynamical theory of nuclear induction, *Physical Review*, 89 (1953) 728.
- [16] J.G. De la Torre, M. Huertas, B. Carrasco, HYDRONMR: prediction of NMR relaxation of globular proteins from atomic-level structures and hydrodynamic calculations, *Journal of Magnetic Resonance*, 147 (2000) 138-146.
- [17] V. Bloomfield, W. Dalton, K. Van Holde, Frictional coefficients of multisubunit structures. I. Theory, *Biopolymers*, 5 (1967) 135-148.